An efficient method to reconstruct invariant manifolds of saddle points

Elisa Francomano[a] · Frank M. Hilker[b] · Marta Paliaga[a] · Ezio Venturino[c]

Communicated by A. De Rossi

Abstract

In vector field analysis, saddle points have two different types of invariant manifolds, namely stable ones and unstable ones. The invariant manifolds represent separatrices that partition the domain of trajectories into invariant regions of different dynamics. In this work, we analyze the basins of attraction of two different stable nodes by reconstructing the separatrices of a saddle point. To this purpose we present a computational algorithm that detects the points lying on the manifold, considering the plane generated by the two stable eigenvectors of the saddle point. Finally we reconstruct the surface by using the moving least-squares approximant method.

1 Introduction

Autonomous systems of ordinary differential equations (ODEs) are a powerful and common tool to model phenomena observed in real life.

These models depend on different parameters, generally describing physical or biological properties; for a particular choice of the parameter values the solutions of the system are the trajectories evolving toward different dynamical scenarios. The set of values approached by the state variables of the system is called *attractor*. Geometrically an attractor could be a single point, a curve, a manifold or even a complicated set with a fractal structure known as strange attractor. However in this work we consider as attractor only a single equilibrium point. In particular we analyze three-dimensional models with two different coexisting stable equilibria, for a given set of parameter values [21]. Therefore, depending on the locations of the initial conditions in the vector field, the solutions of the model will converge to either one of the two attractors.

In this case the trajectory space can be divided into different regions, called *basins of attraction*, which contain all the initial conditions for which the corresponding solution evolves to a specific attractor.

In real-world applications, one of the stable equilibria could be an undesirable configuration of the system. For instance, it could represent the extinction of a species in the ecosystem, the spread of a particular disease in the environment, or the evolution of cancer cells in a patient [22]. Therefore the aim would be to avoid that the system tends toward this equilibrium.

Knowing the vector field features allows to modify the initial conditions in order to reach the alternative attractor. For this purpose many numerical methods have been developed to study the basins of attraction. In [7], [8], [9] the authors propose an algorithm to analyze the surface that divides the different basins of attraction of a two- or three- dimensional model. This surface is called a *separatrix*. To reconstruct the corresponding manifold they take advantage of the Partition of unity meshless method ([10], [12]). Furthermore, many methods for the visualization of the vector field by using the topological characteristic of the critical points have been proposed in the literature. Although these methods are well developed for two-dimensional systems ([5],[17], [20], [23], [25]), only little work exists to analyze three-dimensional models ([16], [24]).

We extend these results and obtain a new numerical method to detect the points on the separatrix surfaces, by using the properties of a particular unstable equilibrium, called *saddle point*.

For each dimension of the state space, a saddle point has two invariant manifolds, one stable and one unstable, which divide the trajectories domain into invariant regions with different dynamics.

We present an algorithm that integrates the scattered points on the stable manifold. Once a suitable number of separatrix points are detected, we reconnect them by using the moving least-squares method presented in [14],[15] avoiding the resolution of a large interpolation system.

This paper is organized as follows. In Section 2 we describe the basic elements and properties of the vector field topology, underling the different classes of the equilibrium points. The numerical tool to detect and reconstruct the separatrix surfaces is presented in Section 3. In Section 4, we present numerical results for attractor basins of an eco-epidemiological model of social predators [18]. Finally, in Section 5, we summarize all the results and some ideas for future work.

[a] Scuola Politecnica, DIID, University of Palermo, Italy
[b] Institute of Environmental Systems Research, School of Mathematics and Computer Science, Osnabrück University, Germany
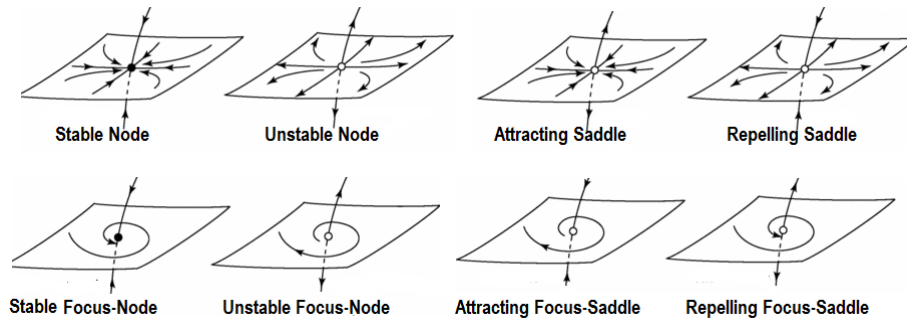[c] Department of Mathematics, "Giuseppe Peano", University of Torino, Italy

Figure 1: Illustration of different classes of equilibrium points in the three-dimensional state space.

2 Vector field topology

Let us consider a three-dimensional dynamical model, generated by a system of ODEs: $\dot{u} = F(u)$ with $u : E \subseteq \mathbb{R}^3 \to \mathbb{R}^3$ and F is a linear or non-linear functional.

An equilibrium point $\mathbf{x}_0 \in \mathbb{R}^3$ is defined as a solution that does not change in time: $\dot{u}(\mathbf{x}_0) = 0$. It is said to be Lyapunov stable [19], if every solution with initial conditions sufficiently close to this point remains close to it:

$$\forall \epsilon > 0 \exists \delta |\mathbf{x} - \mathbf{x}_0| < \delta \implies |\mathbf{x} - \mathbf{x}_0| < \epsilon \ \forall t > 0.$$

The point is asymptotically stable if all the trajectories starting in a neighborhood of the point converge to the equilibrium when $t \to 0$:

$$\forall \epsilon > 0 \exists \delta |\mathbf{x} - \mathbf{x}_0| < \delta \implies lim_{x \to \infty} \mathbf{x} = \mathbf{x}_0 \ , \forall t > 0.$$

In our analysis we consider F as non-linear functional. Therefore the stability of the equilibrium is determined by linearizing the equations of the model about the equilibrium and by looking at the signs of the eigenvalues $\lambda_1, \lambda_2, \lambda_3$ of the Jacobian matrix J. In particular an equilibrium point is *hyperbolic* if the real part of λ_1, λ_2, and λ_3 is not zero.

If all the eigenvalues are real, a critical point could exhibit one of the following features:

Asymptotically Stable Node	$\mathrm{Re}(\lambda_1) < \mathrm{Re}(\lambda_2) < \mathrm{Re}(\lambda_3) < 0$
Unstable Node	$0 < \mathrm{Re}(\lambda_1) < \mathrm{Re}(\lambda_2) < \mathrm{Re}(\lambda_3)$
Repelling Saddle	$\mathrm{Re}(\lambda_1) < 0 < \mathrm{Re}(\lambda_2) < \mathrm{Re}(\lambda_3)$
Attracting Saddle	$\mathrm{Re}(\lambda_1) < \mathrm{Re}(\lambda_2) < 0 < \mathrm{Re}(\lambda_3)$

If the Jacobian matrix J possesses two complex conjugate eigenvalues, the trajectories spiral around the point, and the hyperbolic equilibrium can be classified in the following cases:

Asymptotically Stable Focus-Node	$\mathrm{Re}(\lambda_1) < \mathrm{Re}(\lambda_2) = \mathrm{Re}(\lambda_3) < 0$ $\mathrm{Im}(\lambda_2) = -\mathrm{Im}(\lambda_3)$
Unstable Focus-Node	$0 < \mathrm{Re}(\lambda_1) < \mathrm{Re}(\lambda_2) = \mathrm{Re}(\lambda_3)$ $\mathrm{Im}(\lambda_2) = -\mathrm{Im}(\lambda_3)$
Repelling Focus-Saddle	$\mathrm{Re}(\lambda_1) < 0 < \mathrm{Re}(\lambda_2) = \mathrm{Re}(\lambda_3)$ $\mathrm{Im}(\lambda_2) = -\mathrm{Im}(\lambda_3)$
Attracting Focus-Saddle	$\mathrm{Re}(\lambda_1) = \mathrm{Re}(\lambda_2) < 0 < \mathrm{Re}(\lambda_3)$ $\mathrm{Im}(\lambda_1) = -\mathrm{Im}(\lambda_2)$

These classes of points have different features on the vector field or phase space (Figure 1). The saddle points are always unstable but they are characterized by two different invariant manifolds [21].

Assuming that $\mathbf{x}_s \in \mathbb{R}^3$ is a hyperbolic saddle, the stable manifold $W^s(\mathbf{x}_s)$ has the property that all its orbits tend to the saddle in forward time:

$$W^s(\mathbf{x}_s) = \{\mathbf{x} \in E \,|\, lim_{t \to +\infty} u(\mathbf{x}, t) = \mathbf{x}_s\}.$$

On the other hand, the unstable manifold $W^u(\mathbf{x}_s)$ includes all the trajectories tending to $\mathbf{x}_s$ in backward time:

$$W^u(\mathbf{x}_s) = \{\mathbf{x} \in E \,|\, lim_{t \to -\infty} u(\mathbf{x}, t) = \mathbf{x}_s\}.$$

Therefore the dimension of the stable manifolds is equal to the number of the corresponding eigenvalues.

The manifolds $W^s(\mathbf{x}_s)$ and $W^u(\mathbf{x}_s)$ are fundamental to understand the global behavior of the vector field. In fact they form separatrices, partitioning the state space into invariant regions of different flow behavior, representing the boundaries of the different basins of attraction.

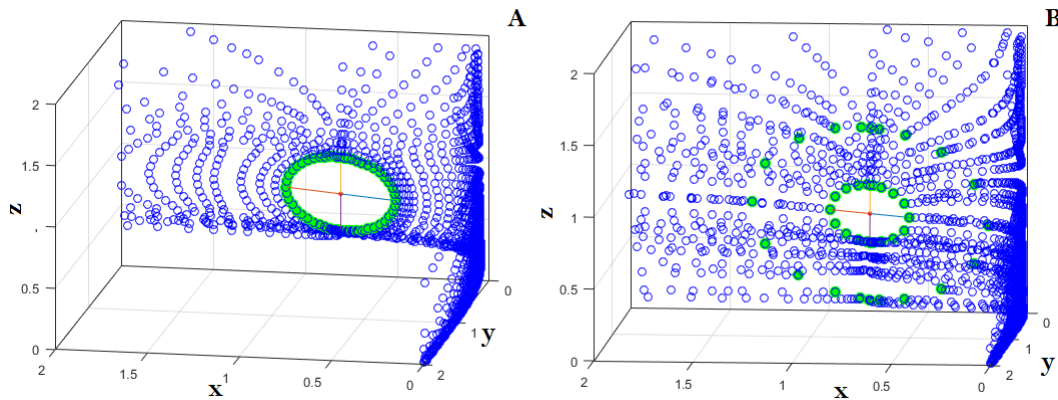In the next section we present a method to detect and reconstruct these manifolds.

Figure 2: Detection of the separatrix points. The green points lying on the ellipses are the initial conditions for backward integration. The blue points are the discrete values of the trajectories. In panel A only one set of seeding points is considered. In panel B two sets are used.

3 Separatrix reconstruction

In the following we illustrate the basic ideas used to approximate the invariant manifolds of the saddle points. We focus our analysis on 3D dynamical models admitting two different stable equilibria. In particular we assume that the system does not have strange attractors or limit cycles, so that the phase space is totally divided into the basins of attraction of the two stable equilibria. We briefly describe the computational approaches adopted in determining the points on the manifolds by employing the characteristics of the saddle points coupled with the integration scheme in generating the separatrix surfaces by avoiding a spatial grid. Namely we will present a moving least squares method that belongs to a particular class of numerical method, called *meshless*, that have gained growing interest in many areas of science ([1],[2], [3], [6],[11], [13]).

3.1 Detection of separatrix points

Let E_1 and E_2 be two stable nodes of a three-dimensional model. As a consequence there exists a saddle point E_s that we assume is attracting. This assumption guarantees the presence of one positive eigenvalue associated to E_s that generates the one-dimensional invariant subspace V^u, which is tangent to the unstable manifold $W^u(E_s)$, while the two eigenvectors v_1 and v_2 associated to the negative eigenvalues generate the invariant subspace V^s, which is tangent to $W^s(E_s)$.

Keeping in mind these positions, we start determining the stable separatrix by considering N equispaced points on a small ellipse, centered at the saddle point and whose semi-axes are the stable eigenvectors v_1 and v_2 (the green points in Figure 2A).

Therefore all these points lie on the subspace V^s and they represent the initial conditions to integrate the manifold. The direction of the integration depends on the topology of the originating saddle. In our case we are studying an attracting saddle; thus we use a backward integration starting from the N initial conditions.

Because the stable manifold is invariant, it means that for each $\mathbf{x}_0 \in W^s$ the solution $t \to u(\mathbf{x}_0, t)$ has its image on W^s. Therefore the orbit passing through each $\mathbf{x}_0 \in W^s$ lies on W^s:

$$\text{if } \mathbf{x}_0 \in W^s \Rightarrow u(\mathbf{x}_0, t) \in W^s, \ \forall t.$$

Therefore we consider as separatrix points the scattered data lying on the trajectories obtained by backward integration (the blue points in Figure 2A).

Sometimes the seeding points might be too close or too far from the saddle point. Specifically in the first case the reconstruction could not be precise because the scattered data are not dense enough, in the second case the part of the manifold close to the saddle is excluded. For these reasons one could rescale the eigenvectors obtaining, on the corresponding ellipses, a different sets of initial conditions.

3.2 Reconstruction of the surfaces

In this section we present a moving least-squares (MLS) method to connect the points found by backward integration.

Given a discrete set $\chi = \{\mathbf{x}_1, ..., \mathbf{x}_N\} \subset \mathbb{R}^d$ of data sites and the respective functional evaluations of f: $\{f(\mathbf{x}_1), ..., f(\mathbf{x}_N)\}$, the idea of this approximation is to solve for each evaluation point $\mathbf{y}$ a locally weighted least-squares problem [26].

The influence of the data are governed by the weight functions $\omega : \Omega \times \Omega \to \mathbb{R}$ that become smaller as the arguments are far from each other. In this work we use radial basis functions that depend on the so-called *shape parameter* ϵ which influences the approximation goodness.

Following the Backus–Gilbert approach [4], we reconstruct the quasi-interpolant

$$P_f(\mathbf{y}) = \sum_{i=1}^{N} f(\mathbf{x}_i)\Phi_i(\mathbf{y}), \tag{1}$$

where $\Phi_i(\mathbf{y}) = \Phi(\mathbf{y}, \mathbf{x}_i)$ are the *generating functions* that govern the approximation goodness. Then the quantity

$$\frac{1}{2}\sum_{i=1}^{N}\Phi_i^2(\mathbf{y})\frac{1}{\omega(\mathbf{x}_i,\mathbf{y})}, \tag{2}$$

has to be minimized with respect to each evaluation point $\mathbf{y}$. To ensure that the quasi-interpolant P_f reproduces polynomials of a certain degree q, the functions Φ_i are subject to the constraints

$$\sum_{i=1}^{N}p(\mathbf{x}_i)\Phi_i(\mathbf{y}) = p(\mathbf{y}) \quad \forall p \in \pi_q^d, \tag{3}$$

where π_q^d is the space of the d-variate polynomials of total degree at most q with dimension $Q = \frac{(d+q)!}{q!d!}$.
The generating functions Φ satisfying (2) and (3) are given by

$$\Phi_i(\mathbf{y}) = \omega(\mathbf{x}_i,\mathbf{y})\sum_{k=1}^{Q}\lambda_k p_k(\mathbf{x}_i), \quad i = 1,...,N, \tag{4}$$

with λ_k being the Lagrange multipliers, i.e. the only solutions of the systems

$$G(\mathbf{y})\lambda(\mathbf{y}) = p(\mathbf{y}), \quad \mathbf{y} \in \mathbb{R}^2, p \in \pi_q^d, \tag{5}$$

where G is the Gram matrix with entries

$$G_{jk}(\mathbf{y}) = < p_j, p_k >_\omega = \sum_{i=1}^{N}p_k(\mathbf{x}_i)p_l(\mathbf{x}_i)\omega(\mathbf{x}_i,\mathbf{y})$$

and $j, k = 1,..,3$.
Thus considering the vector $\Lambda = [\lambda_1,...,\lambda_N]$, and by letting $K(\mathbf{x}_i,\mathbf{y}) = \omega(\mathbf{x}_i,\mathbf{x})\Lambda^T(\mathbf{x})p(\mathbf{x}_i)$, the quasi-interpolant required is:

$$P_f(\mathbf{y}) = \sum_{i=1}^{N}f(\mathbf{x}_i)K(\mathbf{x}_i,\mathbf{y}). \tag{6}$$

Considering the low dimension of the problem and requiring a linear polynomial reproduction, it is possible to find the explicit formula for the Lagrange multipliers:

$$\begin{aligned}
\lambda_1(\mathbf{y}) &= \frac{1}{|G|}(G_{11}^2 - G_{22}G_{33}), \\
\lambda_2(\mathbf{y}) &= \frac{1}{|G|}(G_{12}G_{31} - G_{13}G_{23}), \\
\lambda_3(\mathbf{y}) &= \frac{1}{D}(G_{22}G_{13} - G_{13}G_{23}),
\end{aligned}$$

avoiding the resolution of the systems.
At first glance, this method may appear somewhat scary because it requires the resolution of the Gram system for each evaluation. However the systems are small. In our case the Gram matrix is $G \in \mathbb{R}^{3\times3}$, and as shown it is possible to find the explicit formula for the Lagrange multipliers, thus completely avoiding this problem. In particular, if an elevate number of evaluations is not necessary, this method is efficient and we do not have to solve a large interpolation system [12].
We are now ready to construct the separatrix manifold. We assume the data sites χ as the scattered points projected onto the (n, p) plane, while the data values $f_i = f(\mathbf{x}_i)$ describe the height at $\mathbf{x}_i$. Then we apply the MLS method just described in generating the local approximation.

4   Numerical Results

We show the reconstruction of the separatrix surface using an example that represents an eco-epidemiological system [18]:

$$\begin{aligned}
\frac{dn}{dt} &= r\left(1-\frac{n}{k}\right)n - (1+\alpha p)np, \tag{7}\\
\frac{dp}{dt} &= -(1+\mu i)p + (1+\alpha p)np, \tag{8}\\
\frac{di}{dt} &= i(1-i)(\beta - \mu) - (1+\alpha p)(1-\theta)ni. \tag{9}
\end{aligned}$$

This is the nondimensionalized form of a model that describes the population dynamics of prey and cooperative predators. The population size of prey and predators at time t are denoted by $n = n(t)$ and $p = p(t)$, respectively. Predators suffer an infectious disease, and $i = i(t)$ is the fraction of predators infected. We assume logistic population growth of prey, with k being the carrying capacity and r the intrinsic per-capita growth rate. The time scale of the system has been non-dimensionalized
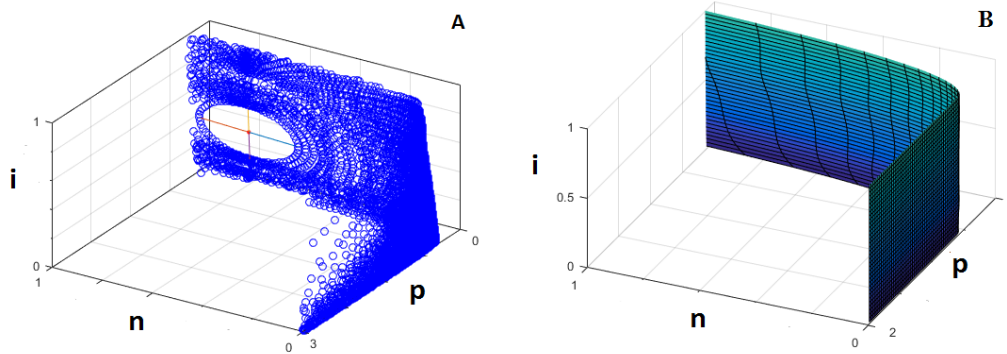
Figure 3: Reconstruction of the separatrix by fixing $r = 10$, $k = 0.8$, $\theta = 0.1$, $\mu = 0.3$, $\alpha = 1.5$, $\beta = 2$. A) Represents all the scattered points obtained with backward integration. B) Represents the approximation of the manifold using the MLS method. Note that while the method in [14, 15] obtained analogous results, it did not include the 'bending' of the separatrix surface that we see here toward larger predator values as the prey population size becomes small.

to represent the average lifetime of predators. Predators grow by consuming prey. The model considers social predators that cooperate in groups when hunting. For instance, lions, wild dogs, and spotted hyenas are known to work together in pursuing their prey. The parameter α represents the strength of cooperation and increases the predator attack rate (which is here scaled to unity). Disease transmission takes place horizontally (between individuals via direct contact) and vertically (from mother to offspring). Horizontal transmission is assumed to be frequency-dependent, with β being the transmission parameter. The parameter $\theta \in [0, 1]$ represents the fraction of offspring acquiring infection from their mother.

Here, we fix the parameter values $r = 10$, $k = 0.8$, $\theta = 0.1$, $\mu = 0.3$, $\alpha = 1.5$, $\beta = 2$, for which the system has the following equilibria: $E_1 \approx (0.8, 0, 0.4061)$ and $E_2 \approx (0.3156, 1.703, 0.4061)$ both stable; $E_0 \approx (0, 0, 0)$, $E_3 \approx (0.8, 0, 0)$ and $E_5 \approx (0, 0, 1)$ all unstable. Finally, the point $E_s \approx (0.7632, 0.3128, 0.4061)$ is an attracting saddle. We integrate the separatrix surface, starting from the attracting saddle E_s and by considering $N = 15$ equispaced points on the plane generated by the two stable eigenvectors $v_1 = (-0.9975; 0.0450; -0.0551)$, $v_2 = (-0.0218; 0.1387; 0.9901)$ rescaled by a factor of 0.2. Then, to have a larger number of points, we have taken another $N_1 = 15$ seeding points on a bigger ellipse, by rescaling the two eigenvectors with a factor of 0.4. Using the Runge–Kutta method (ode45) we integrate backward in time and obtain all the scattered data on the separatrix manifold (Figure 3A), which we reconstruct with the MLS approximant (Figure 3B). As weighted function we use the Wendland C2 compactly supported function centered at the evaluation point $\mathbf{y}$:

$$\omega(\mathbf{x}_i, \mathbf{y}) = (1 - \epsilon ||\mathbf{y} - \mathbf{x}_i||_2)_+^4 (4\epsilon ||\mathbf{y} - \mathbf{x}_i||_2 + 1). \tag{10}$$

The choice of the shape parameter is a crucial factor in the approximation, because it deeply influences the goodness of the results in accuracy. From numerical experiments we obtain that a good choice is $1.5 < \epsilon < 3.5$.

In Figure 3B we show the reconstruction with $\epsilon = 2$ and 70 evaluation points.

The separatrix surface in Figure 3B appears to be independent of the infection level. Moreover, the separatrix takes rather small values of the predator population size. This suggests that predator survival occurs for many initial conditions with large enough predator population sizes because of strong cooperation, as reported in [15]. The separatrix remains unaffected by the supply of prey if the prey population size is large enough. However, if the prey population size approaches zero, the separatrix takes very large predator values. This indicates that more and more initial conditions lead to predator extinction, even with larger initial predator populations. This seems plausible, as predators need prey to survive, no matter how strongly they cooperate in hunting. The method in [14, 15] obtained analogous results. But the new approximation reported in this paper can take advantage of more information and therefore provides a better description of the separatrix. Our present findings indicate that the separatrix surface bends toward higher values of the predators when the prey population becomes small. This feature is new and was not found by the method exposed in [14, 15].

5   Conclusions

In this paper we present an approximation method for the reconstruction of the separatrix. Starting from the previous results [14], [15] we propose an alternative numerical tool to detect the points lying on the surface. Through the analysis of the invariant manifolds of a saddle point we can find the separatrix points by backward integration of the model.

This method turns out to be efficient, and it does not require a high number of seeding points to obtain a good approximation of the surfaces.

This work is a first significant attempt for surface reconstruction, because it has allowed the discovery of a new phenomenon in an ecosystem already investigated, which was not observed using previous algorithms devised for solving the same kind of problems. The results obtained suggest to extend the new methodology to more complex models. Future work could apply the algorithm to detect the scattered data in systems with three or more equilibria or in the presence of periodic orbits.

References

[1] G. Ala, G.E. Fasshauer, E. Francomano, S. Ganci and M.J. McCourt, The method of Fundamental Solutions in solving coupled boundary value problems for M/EEG, SIAM, Journal on Scientific Computing, Vol. 37(4), pp. B570–B590 (2015).

[2] G. Ala, G.E. Fasshauer, E. Francomano, S. Ganci and M.J. McCourt, A meshfree solver for the MEG forward problem, IEEE Transactions on Magnetics, Vol. 51(3), 5000304 (2015).

[3] G. Ala, G.E. Fasshauer, E. Francomano, S. Ganci and M.J. McCourt, An augumented MFS approach for brain activity reconstruction, Mathematics and Computers in Simulation, Article in press, DOI 10.1016/j.matcom.2016.11.009 (2016).

[4] G. Backus and F. Gilbert, The resolving power of gross earth data, Geophys. J. R. Astr. Soc., Vol. 16, pp. 169–205 (1968).

[5] R. Batra and L. Hesselink, Topology based vector field comparison using graph methods, In Proceeding IEEE Visualization '99, pp. 105–114 (1999).

[6] M.D. Buhmann, S. De Marchi and G. Plonka-Hoch, Kernel Functions and Meshless Methods, Dolomites Research Notes on Approximation, 4 (Special Issue), pp. 1–63 (2011).

[7] R. Cavoretto, A. De Rossi, E. Perracchione and E. Venturino, Graphical Representation of Separatrices of Attraction Basins in Two and Three-Dimensional Dynamical Systems, International Journal of Computational Methods, Vol. 14, Issue 1 (2016).

[8] R. Cavoretto, A. De Rossi, E. Perracchione and E. Venturino, Robust Approximation Algorithms for the Detection of Attraction Basins in Dynamical Systems, Journal of Scientific Computing, Vol. 68, pp. 395–415 (2016).

[9] R. Cavoretto, A. De Rossi, E. Perracchione and E. Venturino, Reliable approximation of separatrix manifolds in competition models with safety niches, Int. J. Comput. Math., Vol. 92, pp. 1826–1837 (2015).

[10] A. De Rossi, E. Perracchione and E. Venturino, Fast strategy for PU interpolation: an application for the reconstruction of separatrix manifold, Dolomites Research Notes and Approximation, Vol. 9, pp.3–12 (2016).

[11] F. Dell'Accio and F. Di Tommaso, Scattered data interpolation by Shepard's like methods: classical results and recent advances, Dolomites Research Notes and Approximation, Vol. 9, pp. 32–44 (2016).

[12] G. Fassahuer, Meshfree Approximation Methods with MATLAB, World Scientific Publishing Co., Singapore, pp. 190–205 (2007).

[13] G.E. Fasshauer and M. McCourt, Kernel-based Approximation Methods using MATLAB, Interdiscip. Math. Sci., Vol. 19, World Scientific (2015).

[14] E. Francomano, F.M. Hilker, M. Paliaga and E. Venturino, On Basins of Attraction for a Predator-Prey Model Via Meshless Approximation, AIP Conference Proceedings 1776, NUMTA (2016).

[15] E. Francomano, F.M. Hilker, M. Paliaga and E. Venturino, Separatrix reconstruction studying the Allee effect in a predator-prey model, Applied Mathematics and Computation, submitted (2016).

[16] A. Globus, C. Levitt and T. Lasinski, A tool for visualizing of three dimensional vector field, Proceedings or the 2nd Conference on Visualization '91, pp.33–40 (1991).

[17] J. Helman and L. Hesselink, Visualizing vector field topology in fluid flows, IEEE Computer Graphics and Applications 11 (May), pp.36–46 (1991).

[18] F.M. Hilker, M. Paliaga and E. Venturino, Mathematical modeling of disease spread among cooperating predators, Bulletin of Mathematical Biology, submitted (2017).

[19] A.M. Lyapunov, The general problem of the stability of motion, International Journal of Control, Vol. 55(3), pp.531–773 (1992).

[20] G. Moore, Laguerre approximation of stable manifolds with application to connecting orbits, Mathematics and Computation, Vol. 73, pp. 211-242 (2003).

[21] J.D. Murray, Mathematical Biology I: An Introduction, third edition, Springer, New York (2002).

[22] R. Precup, M.A. Serban and D. Trif, Asymptotic stability for a model of cell dynamics after allogenic bone marrow transplation, Nonlinear Dynamics and Systems Theory, Vol. 13, Issue 1, pp. 79–92 (2013).

[23] H. Theisel and T. Weinkauf, Vector field metrics based on distance measures of first order critical points, Journal of WSCG, Short communication, Vol. 10, pp. 121–128 (2002).

[24] H. Theisel, T. Weinkauf, H.C. Hege and H.P. Seidel, Saddle Connectors- an approach to visualizing the topological skeleton of complex 3D vector fields, Visualization, 2003, IEEE (2003).

[25] X. Tricoche, G. Scheuermann, and H. Hagen, A topology simplification method for 2D vector fields. In Proc. IEEE Visualization, pp. 359–366 (2000).

[26] H. Wendland, Scattered Data Approximation, Cambridge University Press, Cambridge, pp. 35–43 (2010).